On Convection Bands Within Pacific Coast Storms and Their Relation to Storm Structure[1]

ROBERT D. ELLIOTT AND EINAR L. HOVIND

Aerometric Research Inc., Goleta, Calif.

(Manuscript received 13 November 1963, in revised form 13 January 1964)

ABSTRACT

Pacific storms entering Southern California have been intensely sampled and subjected to detailed investigation through a storm study program in the Santa Barbara area during the 1960–63 (inclusive) winter storm seasons.

One result which has emerged from the analyses of precipitation and upper-air data was the discovery that organized convection bands were a common feature within the main precipitation region. These bands were detected from storm precipitation distributions, which, through quasi-objective methods, have been separated into the following three components: storm mean motion precipitation, orographic precipitation, and convection band precipitation.

The typical convection bands appear to be 20 to 40 miles wide, centered some 30 to 60 miles apart, oriented along the upper shear vector (between winds in the convective cloud layers and the adjacent layer above), and moving along a direction of the lower shear vector. There is evidence that the increased convective activity within the bands is associated primarily with the destabilization of the air mass through differential thermal advection.

1. Introduction

Aircraft, satellite, and radar data have revealed the prevalence of banded structure of clouds and precipitation on various meteorological scales in the atmosphere. Kuettner (1959), Malkus (1963), and Winston and Tourville (1961) have pursued this matter in considerable detail with respect to visible cloud patterns. Harper and Beimers (1958) and Boucher and Wexler (1961), among others, have reported on precipitation band-structure in mid-latitude systems.

During the course of the collection and analysis of data in the Santa Barbara area in connection with a study of the water balance of winter storms, a renewed effort was made to shed more light upon the mesoscale band-structure within storm systems. Numerous extra rawinsonde ascents were made during four years of winter storm sampling at five locations in the area extending eastward from the U. S. Naval Missile Center Facilities at Point Arguello (PGU) and San Nicolas Island (NSI) to the U. S. Weather Bureau station at Santa Monica (LAX). Many of these were made with a frequency of one every three hours, and some at Santa Monica were made hourly.

In addition, extensive flight observations of cloud-water content and other variables were made over the triangular area, and a special recording raingage network provided rainfall data from the boundary coastal plains and mountains, with a few observations from the Santa Barbara Channel Islands. Radar observations were also made at Santa Barbara Airport. The general layout of sounding stations and recording raingages is shown in Fig. 1.

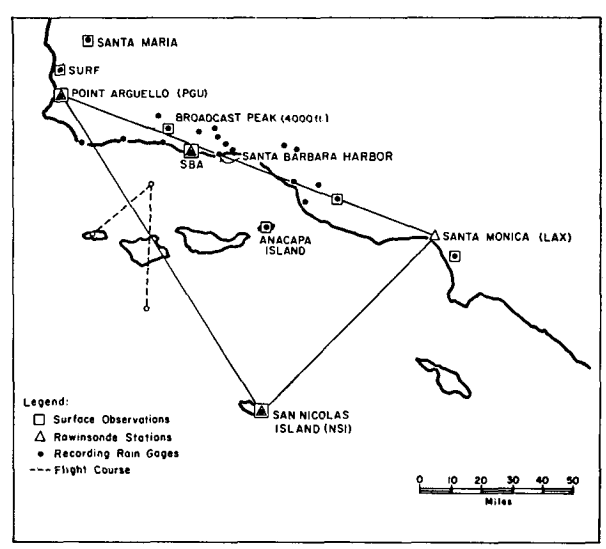

FIG. 1. Map of the storm sampling area.

[1] The results reported herein constitute a portion of the work accomplished under National Science Foundation Contract C-104, Investigation of Cloud-Water Budget of Pacific Storms. R. D. Elliott and E. L. Hovind are co-principal investigators.

2. Analysis of aerological data

The storms passing through the sampling triangle were generally the southward extensions of the frontal zones of cyclonic centers moving into northern California and Oregon. The four storm units discussed in this paper exhibited no important changes in trough intensity or movement during their passage through the sampling area. Therefore, they were considered to be quasi-steady state systems with a fixed translation velocity. Time cross sections are therefore a convenient tool in their analysis since the time scale can be translated into space by means of the system velocity. Furthermore, computed vertical velocities can be employed together with the horizontal velocities relative to the moving system to form streamlines in a vertical time-space section, thus providing a graphic picture of the low-level convergence toward the frontal zone and other flow features.

Two different kinematic methods were employed in the computation of horizontal divergence and, therefrom, the vertical motion. One is based upon the synoptic rawinsonde triangle Pt. Arguello, Santa Monica, San Nicolas Island (see Fig. 1) and is hereafter referred to as the Triangle Method. The other combines the rawinsonde data at two of these stations with the relative movement of the storm system. This kinematic type analysis is hereafter referred to as the Rectangle Method. To minimize any orographically induced effect upon the divergence computations by either method, an appropriate low-level wind correction has been applied at times to the Point Arguello winds.[2]

This mesoscale rawinsonde triangle, which comprises an area of approximately 12,000 km^2, is unique for the west coast of the United States since it is situated over water with the center some 30 statute miles offshore. During storm conditions near-synchronous balloon positions at the vertices of the triangle were obtained from the original U. S. Weather Bureau rawinsonde computation charts (WBAN-20), from which the areal changes with height of the initial triangle could be computed. These computations were carried out at 500-m increments up to the 3000-m level and at 1000-m increments above. From vertical integration of the smoothed horizontal mass divergence field, the distribution of vertical motion with height was determined.

The triangle computations are limited to the times when near synchronous observations are available from the three stations. Because soundings at NSI were seldom taken at less than six-hourly intervals, this also became the time limit of successive triangle computations. In order to employ the three-hourly soundings at the other stations, the Rectangle Method was devised.

[2] This correction resulted from a synoptic-climatological wind study at Point Arguello, located at the west end of the east-west oriented Santa Ynez mountain range, where a terrain-induced acceleration was found of the flow out of the southeast quadrant below 2000 m.

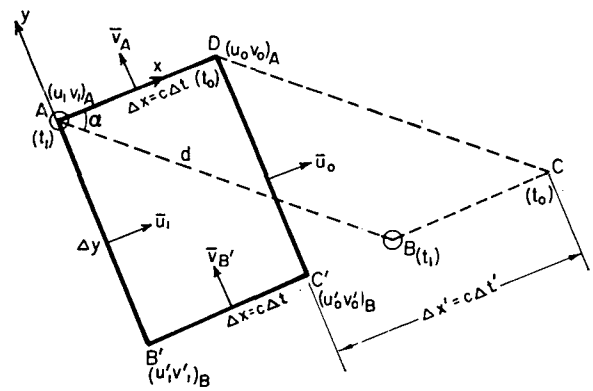

FIG. 2. Rectangle area $AB'C'D$ in relation to the rawinsonde stations A and B used in horizontal divergence computation. The storm system moves in the x-direction with a speed c, and with the base line AB sweeping an area $ABCD$ during a time increment Δt. The rectangle area is obtained by applying a time-shift $\Delta t'$ to station B. The horizontal wind components u and v are in the x and y directions, respectively.

Its essence is depicted schematically in Fig. 2 and is described below.

Let A and B be two rawinsonde stations separated by a distance d. The storm system is assumed to move with a constant speed c in the direction x, which intersects the base line AB at an angle α, while y is the direction perpendicular to x. The horizontal wind components u and v are in the x and y directions, respectively. Furthermore, t_0 and t_1 are the times of successive rawinsonde observations during which time increment (Δt) the system has moved a distance $\Delta x = c\Delta t$.

The horizontal mass divergence can now be computed from the parallelogram ABCD However, since the physical systems roughly paralleled the y-axis, it was felt that a more consistent computation could be derived from the use of the rectangle $AB'C'D$. The winds at B' and C' were obtained from a proper interpolation of the sequential wind observations at station B over the necessary time shift $\Delta t' = \Delta x' c^{-1}$. (See Fig. 2).

From the kinematic expression of horizontal mass divergence in a finite form, we then have:

$$\mathrm{Div}_H \mathbf{V} \simeq \frac{\bar{u}_0 - \bar{u}_1}{\Delta x} + \frac{\bar{v}_A - \bar{v}_{B'}}{\Delta y} \tag{1}$$

where

$$\bar{u}_0 = \frac{(u_A + u_{B'})_0}{2}; \quad \bar{u}_1 = \frac{(u_A + u_{B'})_1}{2};$$

$$\bar{v}_A = \frac{(v_0 + v_1)_A}{2}; \quad \bar{v}_{B'} = \frac{(v_0 + v_1)_{B'}}{2};$$

$$\Delta x = c\Delta t; \quad \Delta y = d \sin\alpha; \quad \Delta t = t_0 - t_1;$$

with the subscripts referring to the aforementioned observation times and stations.

According to the principle of conservation of mass, the horizontal divergence can also be expressed as

$$\mathrm{Div}_H \mathbf{V} = -\frac{\partial \omega}{\partial p} \quad , \tag{2}$$

where p is pressure and ω the vertical motion expressed in pressure units.

Employing Eq (2) and (1) and integrating between the two isobaric surfaces p_0 and p_1 (p_0 the lower surface) we have the vertical motion at the isobaric surface p_1 expressed as:

$$\omega_1 = \omega_0 + \overline{\mathrm{Div}_H \mathbf{V}}(p_1 - p_0), \tag{3}$$

where $\overline{\mathrm{Div}_H \mathbf{V}}$ represents the mean divergence of the air column bounded by the two isobaric surfaces.

A special case of the Rectangle Method arises when the angle α is zero. The system is then moving along the base line AB and only the x-term of Eq (1) can be computed. If one assumes that the y-term is negligible and, furthermore, applies the method to a single station with the conventional time-space exchange, one has in essence the method used by Clarke (1961) in his mesoscale study of dry fronts.

In applying the Rectangle Method to the storms discussed below (Figs. 3–6) the wind data were taken from the WBAN-31 charts at the standard 50-mb levels, where the wind direction is given to the nearest degree and the speed to the nearest m sec^{-1}. For all the storms, Pt. Arguello–Santa Monica was used as baseline AB with $d = 209.4$ km, except for the storm of 16–17 March, 1963, when San Nicolas Island–Santa Monica was used, for which $d = 127.5$ km. A three-point smoothing (over 150-mb depth) of the computed divergence values was made before the vertical integration was performed.

As to the relative accuracy of the Triangle and Rectangle Methods, the former is considered to give more representative values of the non-orographic divergence and vertical motion field in the area of investigation. It utilizes observed balloon positions in space, and although it assumes the wind field between the vertices of the triangle to be a linear function of space, as does the Rectangle Method, it requires no assumption of a steady-state system moving with a constant velocity, and measures, in effect, a quasi-instantaneous average over a slowly shifting triangle. The Rectangle Method measures a time average over a number of hours and over the projected area. However, in the following discussion of four selected storms, it will be seen that the two methods do give comparable results, which support the use of the Rectangle Method as a means of adding resolution to the analysis.

In order to depict the relationship between the precipitation distribution, air mass stability, and air mass flow relative to moving frontal systems, vertical time sections have been prepared for the four storms and are presented in Figs. 3–6. The time-dependent quantities (i.e., precipitation, winds, etc.) for the two rawinsonde stations A and B (see Fig. 2) have been plotted relative to the time of frontal passage at the mid-point between the two stations, with the relative low-level winds based upon the reported 1000-mb wind. In most cases this level was above the ground; when it was not, however, the relative low-level wind vector was given by $-\mathbf{c}$. The precipitation is represented as rate of rainfall in inches per hour, determined from the recording raingage records using 15-min precipitation increments.

The indicated air mass stability represents the mean condition between A and B. The convective instability layers have been outlined with continuous lines of CIB (Convective Instability Base) and CIT (Convective Instability Top). Within these layers, the observed lapse-rate equals or exceeds the saturation adiabats where convective buildups could take place whenever a low-level lift provides enough moisture for convective instability to be realized. From detailed examination of numerous rawinsondes taken during storms in association with aerial and radar observations, it has become apparent that the reported dewpoint deficit alone will not adequately describe the existing cloud conditions. Ascending balloons may rise through clear regions between upper cloud towers as often as they may penetrate the full extent of the towers or just slice through them. Furthermore, the lithium chloride humidity elements which are still in general use are subject to lag, polarization effects, and washouts, which tend to reduce their effectiveness in the upper cloud layers. The combined effect may be a recorded moisture field having little resemblance to the actual cloud-top distribution. The latter appears better defined by means of the top of the potential convective cloud layer (CIT).

The indicated streamlines in Figs. 3–6 have been determined from the relative wind component $(u-c)$ and the vertical motion (w) with the slope of the streamlines β in the vertical section given as

$$\beta = \tan^{-1} k \frac{u-c}{w}.$$

Here k is a scale factor based on the ratio of the horizontal to the vertical scale of the time section.

The vector arrows represent the resultant vector wind between $(u-c)$ and (w), with single stroke arrows referring to vertical motion computations by the Rectangle Method, and the double-stroke arrows by the Triangle Method. The streamline patterns have been drawn to the best fit of both types of wind vectors, but with preference to the triangle computations whenever the two methods gave conflicting results. This, however, occurred rather seldom, as can be seen from the time sections.

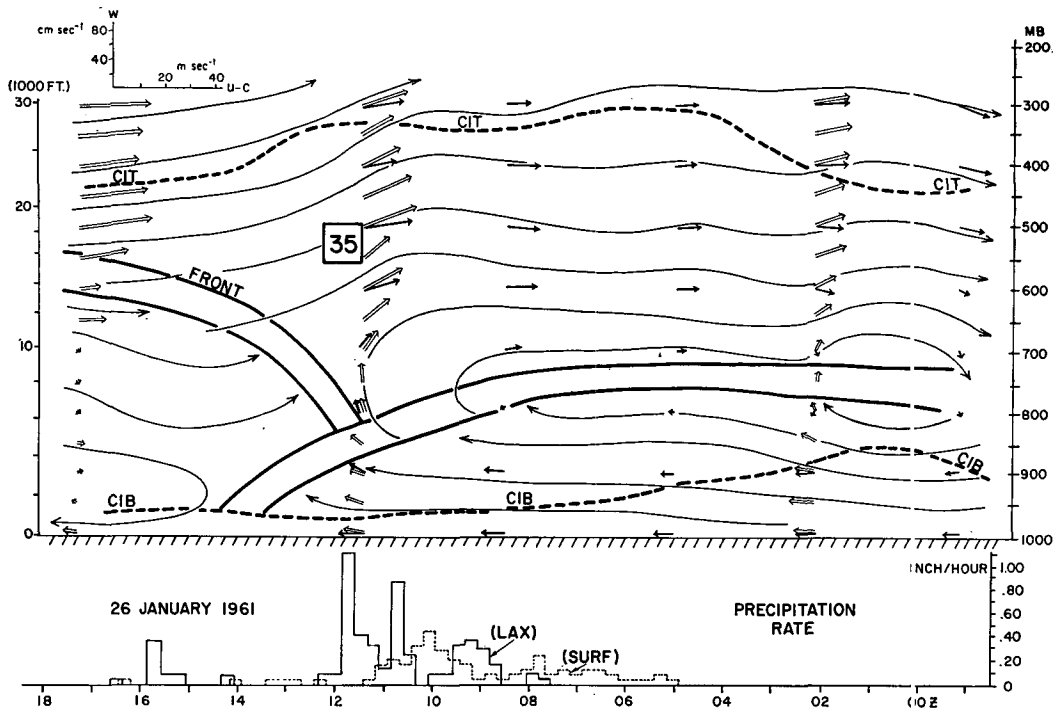

FIG. 3. Time section 26 January 1961. A vertical section in the plane along the direction of movement of the system with precipitation rates (inches per hour) relative to the frontal passage (frontal surfaces thick heavy lines). The mean convective cloud layers are outlined (heavy broken lines) as base (*CIB*) and top (*CIT*) of the convective instability layers. The relative streamlines (thin solid lines) are based upon the horizontal relative wind component ($u-c$) and the vertical motion (w) computed either by the Triangle Method (double-stroke vectors) or Rectangle Method (single-stroke vectors), with the horizontal and vertical scales indicated on top of the time section.

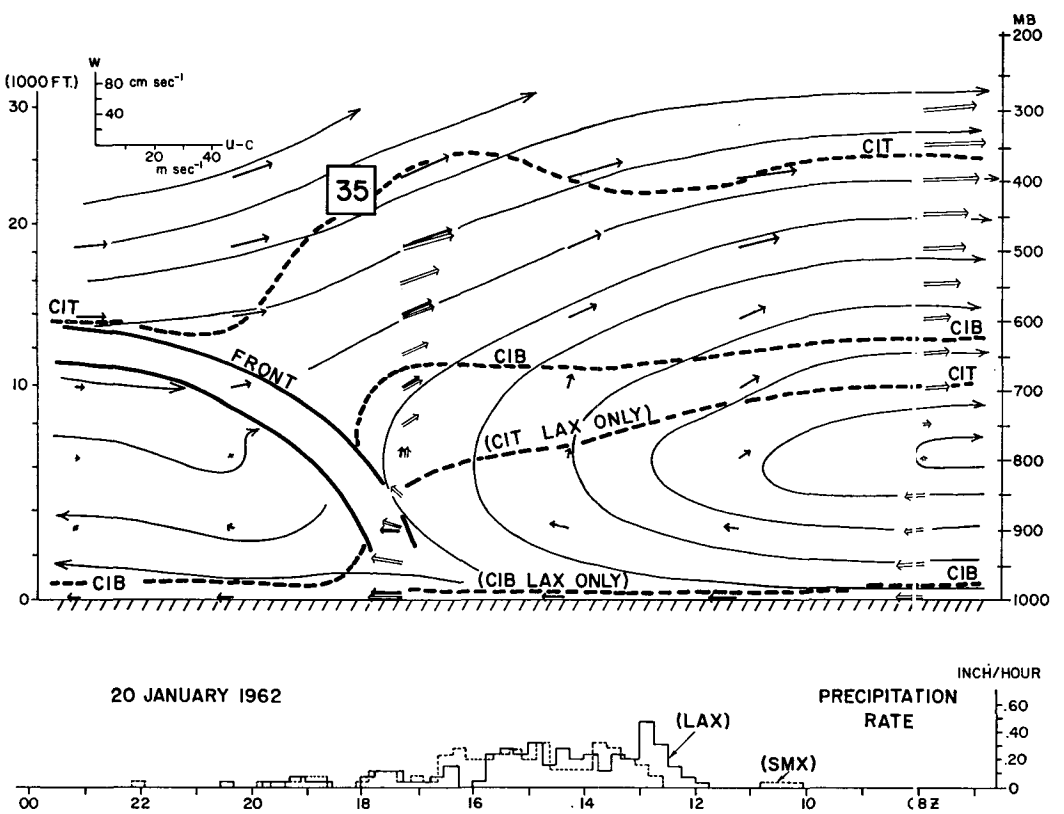

FIG. 4. Time section 20 January 1962. Symbols as in Fig. 3.

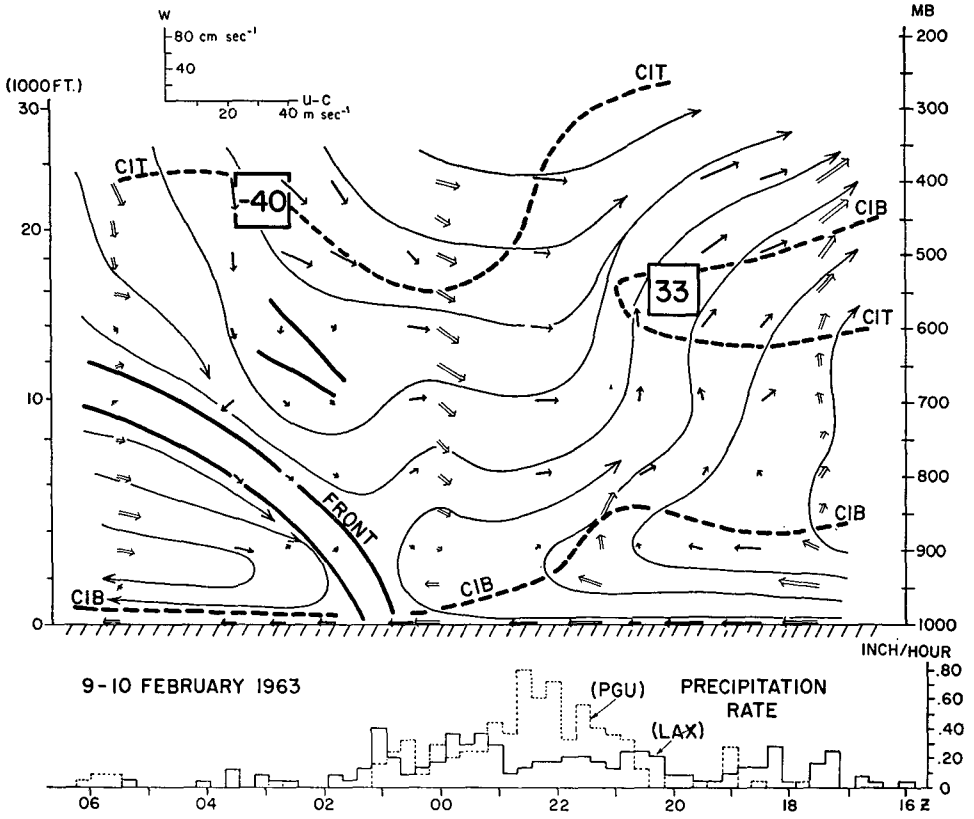

FIG. 5. Time section 9–10 February 1963. Symbols as in Fig. 3.

Finally, the areas of maximum vertical motion have been indicated on the sections with "boxed" numbers with magnitude in cm sec^{-1}. When these relative streamline patterns are considered it must be remembered that they are two-dimensional representations of the flow. Actually, the wind field in Figs. 3–6 had an appreciable v-component into the plane (in the positive y-direction), and the frontal surfaces also sloped upward in the same direction. With this three-dimensional picture in mind the pronounced pre-frontal air mass lifting, suggested by the streamlines in all four storms, can be visualized as taking place along a half-helical path with a clockwise sense in the direction of motion. This lifting or overturning of the air mass is seen to coincide with regions of marked deepening of the convective cloud layers as well as with periods of heavier precipitation, where analysis indicated a puncturing of the weak warm-frontal surfaces or low-level inversions by convection.

3. Analysis of rainfall data

Calculations of storm mean upward motion by methods described above show that midtropospheric vertical velocities of 10 cm sec^{-1} were frequent, with peak values for short periods rising to 30 cm sec^{-1} or more. These vertical velocities were larger than the values computed by numerical methods and received from the U. S. Weather Bureau's National Meteorological Center for the same storms, but could still not account for some of the higher intensities of precipitation observed at non-orographic stations within the raingage network.

Much variability of precipitation intensities was found during storms with hourly rates characteristically varying from several hundredths of an inch per hour to several tenths of an inch per hour over periods of an hour or two. The precipitation rates entered on the four time sections exemplify this effect. The short-period fluctuations suggest the presence of convective showers embedded within the general storm cloud and precipitation complex. By comparing records from surrounding stations, it was discovered that the bursts were not randomly distributed spacewise and timewise, as is often the case in summer showery weather, but were organized in lines or bands which swept eastward through the area. Each band could be traced for over a hundred miles.

From extensive analyses of the network rainfall data on a 15-minute time resolution, it was found possible to separate by quasi-objective methods the following three precipitation components:

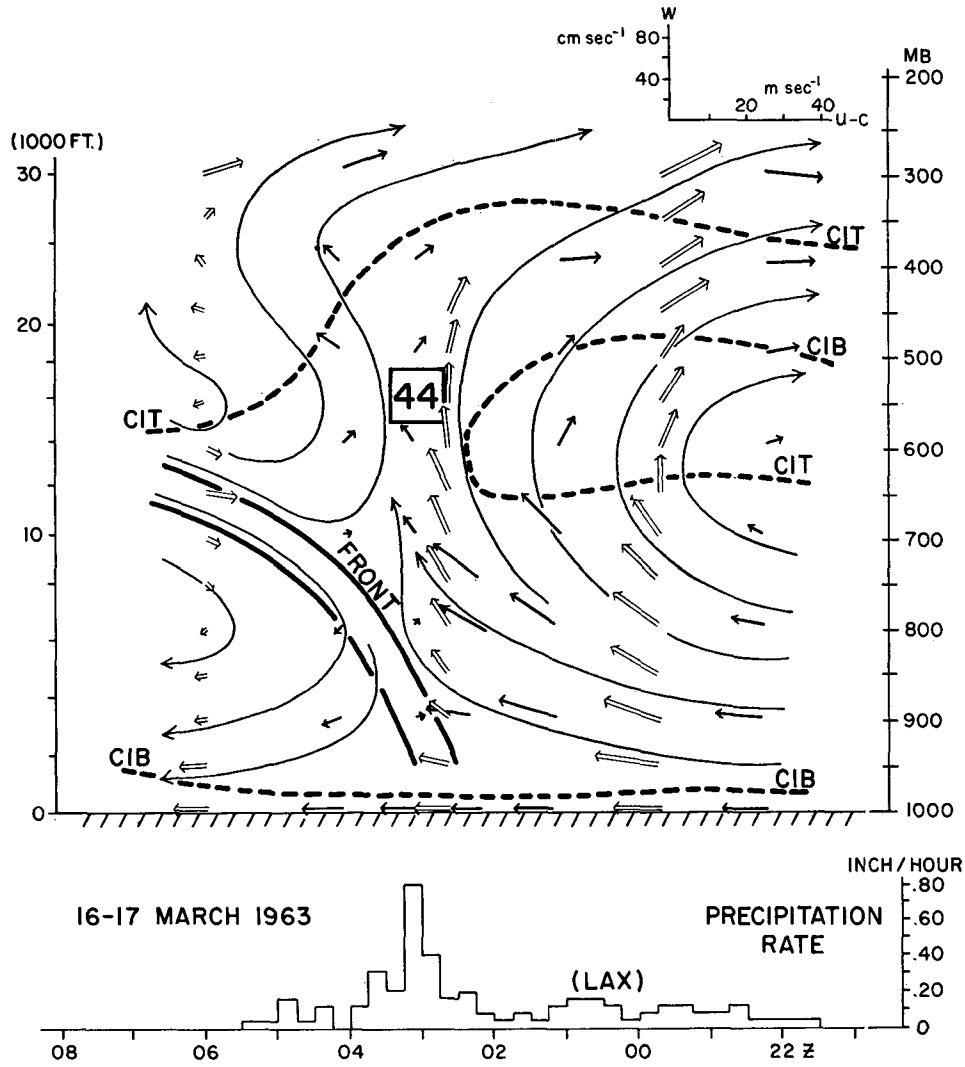

FIG. 6. Time section 16–17 March 1963. Symbols as in Fig. 3.

1) A "storm mean convergence motion" precipitation rate which is the result of the large scale air-mass lifting, as best computed from the rawinsonde triangle data.
2) An "orographic" precipitation rate, the magnitude of which will depend upon the station's location relative to topographic features, and upon air flow, as well as upon the air-mass stability.
3) A "convection band" precipitation rate which is superimposed upon the others and is associated with convective overturning plus the convergence field of moving convection bands within the storm system.

An example of such precipitation analysis from the storm of 20 January 1962 is shown in Fig. 7. Here the precipitation rates for the stations Santa Maria, Broadcast Peak, Santa Barbara Harbor, and Anacapa Island, all along an 85-mile cross section through the sampling area, have been plotted against time. The various components of the precipitation rates have been indicated.

The storm mean motion component, as best seen at the non-orographic stations Santa Maria, Santa Barbara Harbor, and Anacapa Island, was between 0.05–0.10 inch per hour, and constitutes about 25–30 per cent of the total precipitation at these stations. The remaining 70–75 per cent was concentrated in the convection-band precipitation with magnitudes up to 0.20–0.30 inch per hour. This ratio differs for stations with marked orographic precipitation as seen at Broadcast Peak (4000 ft msl) in Fig. 7. Whereas the storm mean motion component for this station remained near 25 per cent, the convection-band component was about 20 per cent of the storm total, while around 55 per cent was connected with orographic precipitation of magnitudes up to 0.30 inch per hour.

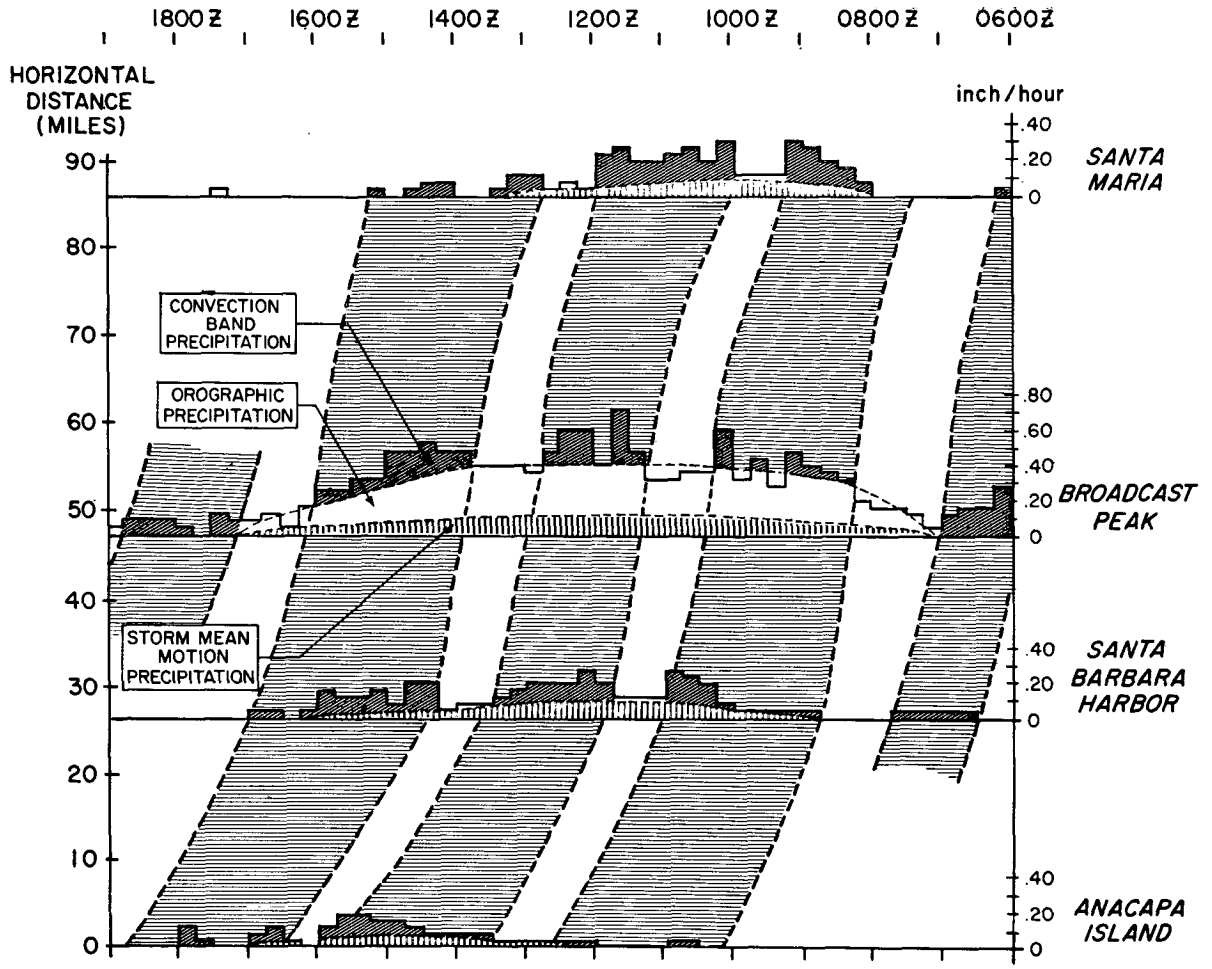

FIG. 7. Precipitation distribution from 20 January 1962, at four stations along an 85-mile cross section (see Fig. 1). The storm total precipitation is separated into three components: the storm mean motion precipitation (vertical hatching), convection band precipitation (diagonal hatching), and orographic precipitation, as seen at Broadcast Peak (4000 ft msl). The time-spatial distribution of convection bands is marked with horizontal hatching.

Several distinct convection bands were found within this storm system. Fig. 7 shows these bands to have a speed component along the cross-section of about 25 mph with widths varying between 30 and 50 miles.

4. Relation of convection bands to storm structure

The movement and orientation of convection bands relative to the upper flow have been subject to several investigations in recent years. Harper and Beimers (1958) studied movement of "precipitation belts" in England and found that they correlated best with the mean wind component across the belts at the 700-mb level, which they suggested to be closest to the "steering level" for these belts. Boucher and Wexler (1961) also found good correlation between the motion of "precipitation lines" and the 700-mb wind component in their direction of motion in the Midwestern and New England areas. They showed the direction of motion to be within 10 to 70 deg and 50 to 90 deg to the right of the 700-mb wind direction for the two areas, respectively.

The aerial arrangement of convection bands as analyzed from the four storms of 25–26 January 1961, 20 January 1962, 9–10 February 1963, and 16–17 March 1963, is shown for selected times in Fig. 8. The individual band movements were obtained from detailed isochrone analysis over the raingage network. The overall direction of motion for each band, effectively from left to right in Fig. 8 and perpendicular to the band, was estimated to the nearest degree. The angular deviation from the representative 10,000-ft wind, as obtained from the sequential three-hourly rawinsondes, as well as the band speed was computed for each band. The number of bands for each storm, their mean speed, and their mean angular deviation from the 10,000-ft wind are summarized in Table 1, where results from a number of bands tracked by similar methods in other parts of the United States[3] are also included. On the average, the bands are seen to move along a direction with a mean deviation to the right of the 10,000-ft wind which agrees well with the findings mentioned above. The band

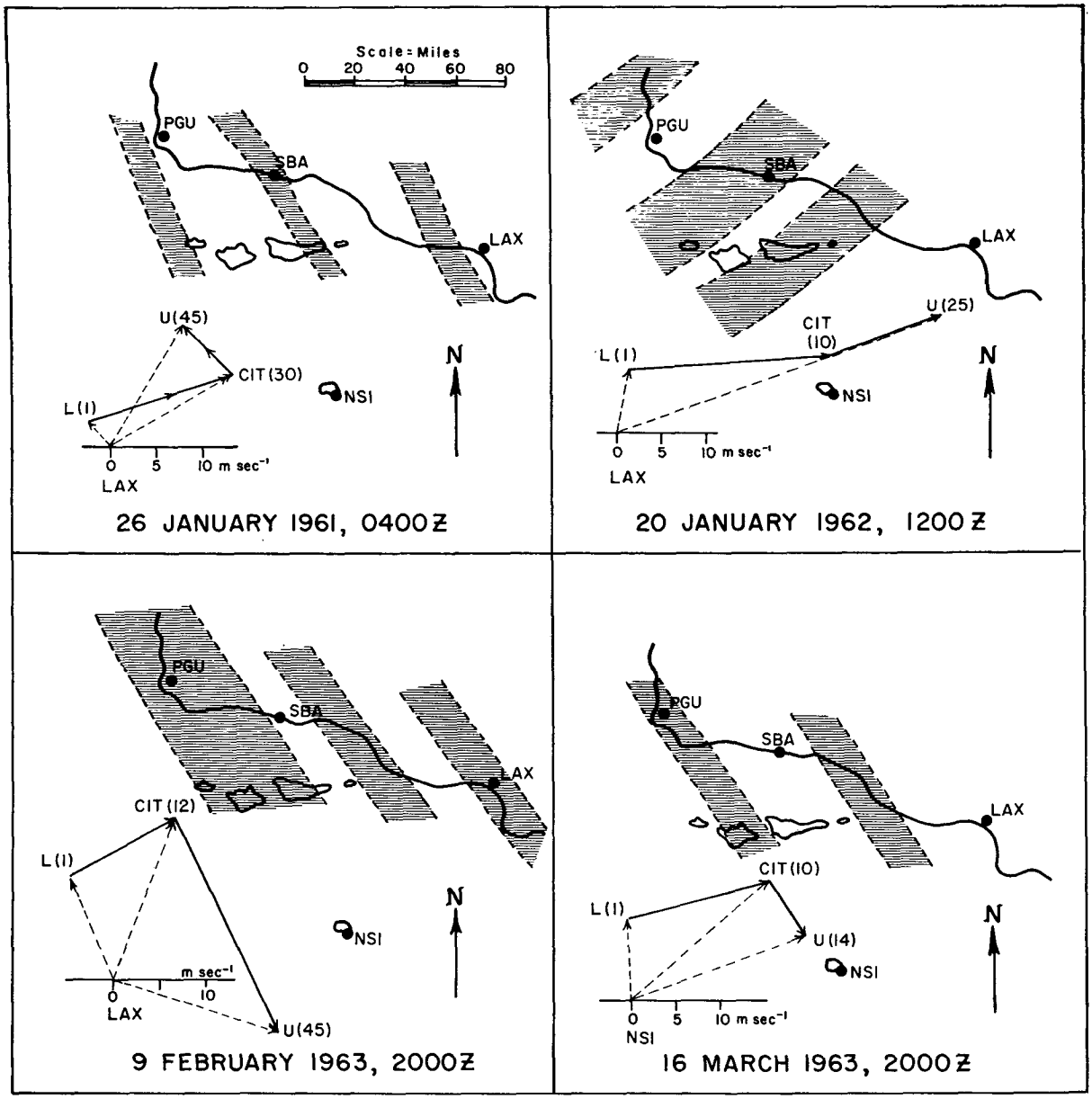

FIG. 8. Geographical distribution of convection bands (horizontal hatching) and their orientation relative to the upper flow for four separate storms. The wind vectors and shear vectors are indicated in dotted and solid lines, respectively. *L* is the low-level wind, *CIT* the wind near the top of the convective cloud layer, and *U* the upper wind in the layer above. The numbers refer to height in thousands of feet.

speed was generally somewhat slower than the wind component normal to the bands at this level.

These convection bands, all embedded within precipitation areas of extratropical cyclones, appear therefore to have a definite crosswind orientation relative to the flow in the lower troposphere. It is hypothesized here that the formation and orientation of these bands are associated with the wind-shear between the convective cloud layer and its upper boundary in a manner similar to that suggested by Malkus (1963) for the occurrence of highly organized cloud rows over the tropical oceans. The latter has a predominant mode parallel to the trade winds, according to Malkus, since the convective cloud layers in the tropics are mostly embedded within the trade winds. However, when they extend up into the stronger shear zones aloft, which is the usual condition in middle latitudes, a crosswind mode may dominate, as was also demonstrated by Malkus for the tropical oceans. This is illustrated in Fig. 8 by the shears between the convective cloud layer and its upper and lower

TABLE 1. Movement of convection bands relative to 10,000-ft wind.

Storm area and date	No. of bands	Band movement: Mean speed (kts)	Band movement: Mean angular deviation from 10,000-ft wind (deg)
Santa Barbara, Calif.			
25–26 January 1961	6	19	45
20 January 1962	5	22	42
9–10 February 1963	5	15	38
16–17 March 1963	2	14	33
Los Angeles, Calif.			
8 and 11 February 1962	11	18	15
Atlanta, Ga.			
18–19 February 1962	4	28	41
Seattle, Wash.			
6 April 1962	3	31	13
Chicago, Ill.			
28 April 1962	5	21	16

boundaries which have been entered for the four storms discussed above. In all cases, the convection bands paralleled the upper shear, while the lower shear showed a strong cross-band component, suggesting an association with the overall steering of these bands.

A complete physical model of these convection bands has not yet been advanced to a point where a mathematical treatment of the dynamics of their development and propagation can be presented. Attempts to relate these systems to microbarographic fluctuations have succeeded only to a limited extent.

The typical bands studied were 20 to 40 miles wide and centered 30 to 60 miles apart (Malkus found a 40-mile cross-mode spacing of the cloud rows in the tropics). The internal structure of the bands consisted of convective cells, apparently randomly arranged, having an appreciable motion relative to the bands and towards the low pressure end of the bands.

A further insight into the cellular structure of the bands is provided by the results from a rate of rainfall recorder[4] which was used during the 1963 storm season. A sample of the standard recording raingage chart and the corresponding rate of rainfall recording chart is given in Fig. 9. The cellular structure is clearly seen in the latter where significant changes in precipitation rates occurred over a period of minutes. From the duration of precipitation peaks and the average rate of translation of cells from a number of cases studied, the diameter of the precipitation cells appears to be of the order of 2–4 miles. The individual cells are short lived but provide the brightest radar echoes and the bulk of precipitation, according to radar observations at Santa Barbara Airport. It is the envelope of these cells that constitutes the boundaries of the bands which exist as identifiable and trackable entities for up to three hours or about 100 miles. It is hypothesized that within these bands, in contrast to the between-band regions, convective momentum transport is strong enough to establish supergradient winds at lower levels and subgradient winds aloft. The resultant field of acceleration would produce horizontal divergence patterns along the leading and trailing edges of the bands, giving upward motion in advance of the bands with downward motion to the rear. However, this circulation could not be detected by the triangle or rectangle computations (see Figs. 3 and 4).

On the other hand, the increased convective scale vertical motion within these bands has been observed with the instrumented aircraft used during the storm study project, particularly on the storm of 20 January 1962,[5] when penetration of the convection bands depicted in Fig. 7 showed significant differences in cloud structure, liquid-water-content values, and turbulence between regions inside and outside the bands. The energy for this convective motion is derived from the net buoyancy of all the cells. Because the effect of surface and radiational heating and cooling was found to be relatively small for the storms sampled, it is postulated here that the increased convection within the bands is associated primarily with the destabilizing effect produced by differential thermal advection. Several investigators, among them Showalter (1944), Smith (1950), Chapman and Carr (1952), and Appleby (1954) have demonstrated an association between this process and high intensity precipitation. Miller (1955) also verified this relationship for a number of storms over small areas and for short periods. The stability of the atmosphere will also be affected by vertical air-mass stretching, whereby differential vertical motion will tend to establish neutral stability. The vertical stretching will have a destabilizing effect upon an initially moist, stable air mass by making the existing lapse rate approach the saturation adiabats, but will, in a similar manner, have a stabilizing effect upon a moist, unstable air mass.

The above effects have been evaluated for the four storms under study and are depicted graphically in Fig. 10 as instability indices, together with the gross precipitation features of the storms. The indices were determined as follows:

i) Under the geostrophic assumption, the thermal advection through a finite layer is proportional to the area on the hodograph bounded by the lower and upper

[3] Elliott, R. D., R. E. Kerr, Jr., E. L. Hovind, J. G. Cronin and J. R. Thompson: Mesoscale analysis of existing meteorological network data. Final Report, U. S. Weather Bureau, Contract Cwb-10326, 162 pp.

[4] This instrument was developed by Aerometric Research Inc. for this project along the principles of Jardi as discussed by Middleton (1947).

[5] Elliott, R. D., E. L. Hovind and J. W. Flavin, Jr.: Investigation of cloud-water budget of Pacific storms. Final Report, National Science Foundation Contract C-104, 64 pp.

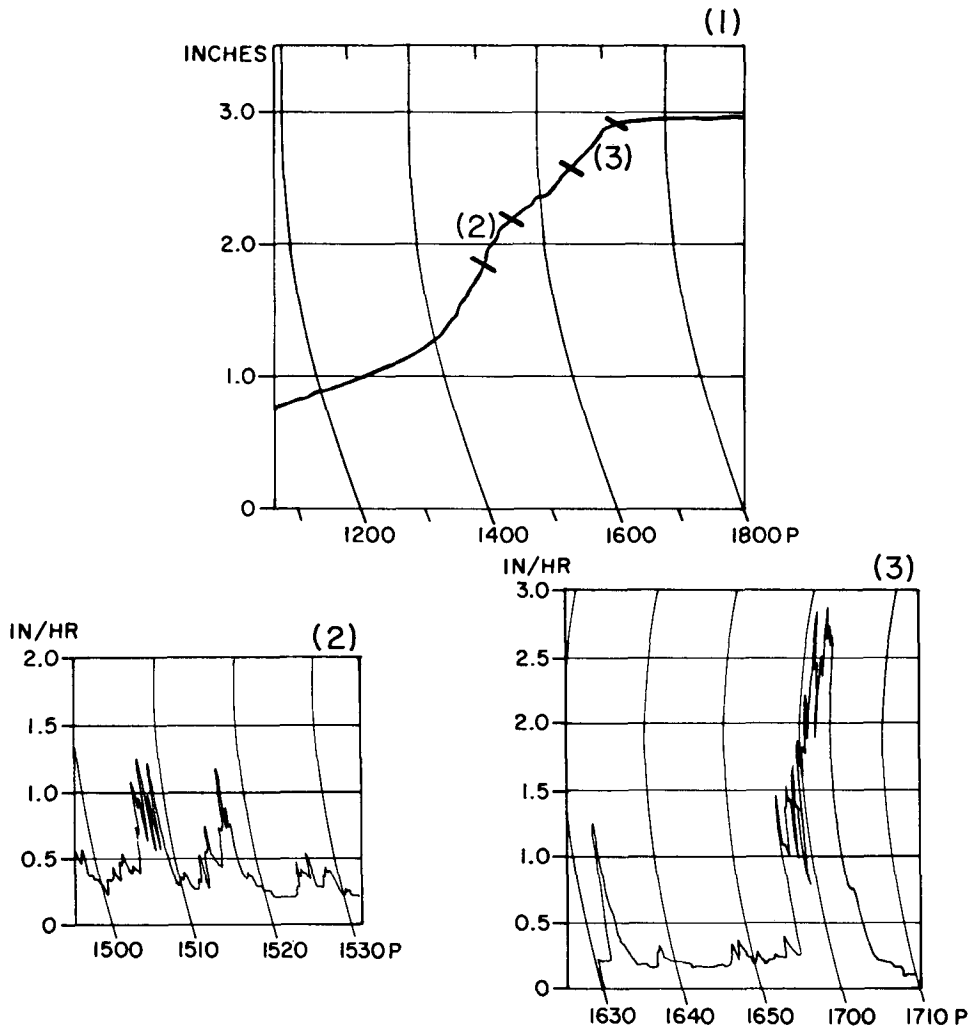

FIG. 9. Precipitation records from Santa Barbara Airport, 16 March 1963. The rate of rainfall records in (2) and (3) are for selected periods as indicated on the recording raingage record (1).

wind vectors and by the shear vector. Thus, for each sounding, the areas associated with maximum thermal advection in the lower layers and with the thermal advection in the adjacent layer above have been evaluated. The frictional layer from surface to 2000 ft has been excluded in these computations. The index as plotted in Fig. 10 represents the rate of change of area with height where positive values indicate the destabilizing effect resulting from, for example, warm air advection in the lower layer and cold air advection above. The scale is arbitrary; however, an index of 15, which was among the higher values observed, corresponds to a change in lapse rate of about $1.5C \cdot 3000\ m^{-1}\ hr^{-1}$, a sizeable value.

ii) The vertical stretching of the air column is represented by two indices computed from the triangle scale vertical motion field: one low-level index for the region below 700 mb, the other for the adjacent region above up to 500 mb. The scale represents the air-mass stretching in cm sec^{-1} cb^{-1}. As mentioned above, the destabilizing effect depends upon the initial stability of the air mass; however, computations using the extremes in observed lapse rates for these storms with an index of 10, give a change in lapse rate of less than $\pm 0.5C \cdot 3000\ m^{-1}\ hr^{-1}$. This is appreciably less than the effect of differential thermal advection.

The results in Fig. 10 are based upon the Santa Monica data from the storms depicted in Figs. 3–6. The outstanding feature is the prominent increase in the differential advection just prior to and/or during the periods of increased precipitation. The vertical stretching effect also displays a definite pattern, usually with a reversal in sign after the onset of precipitation; however, its effect must be considered in regard to the

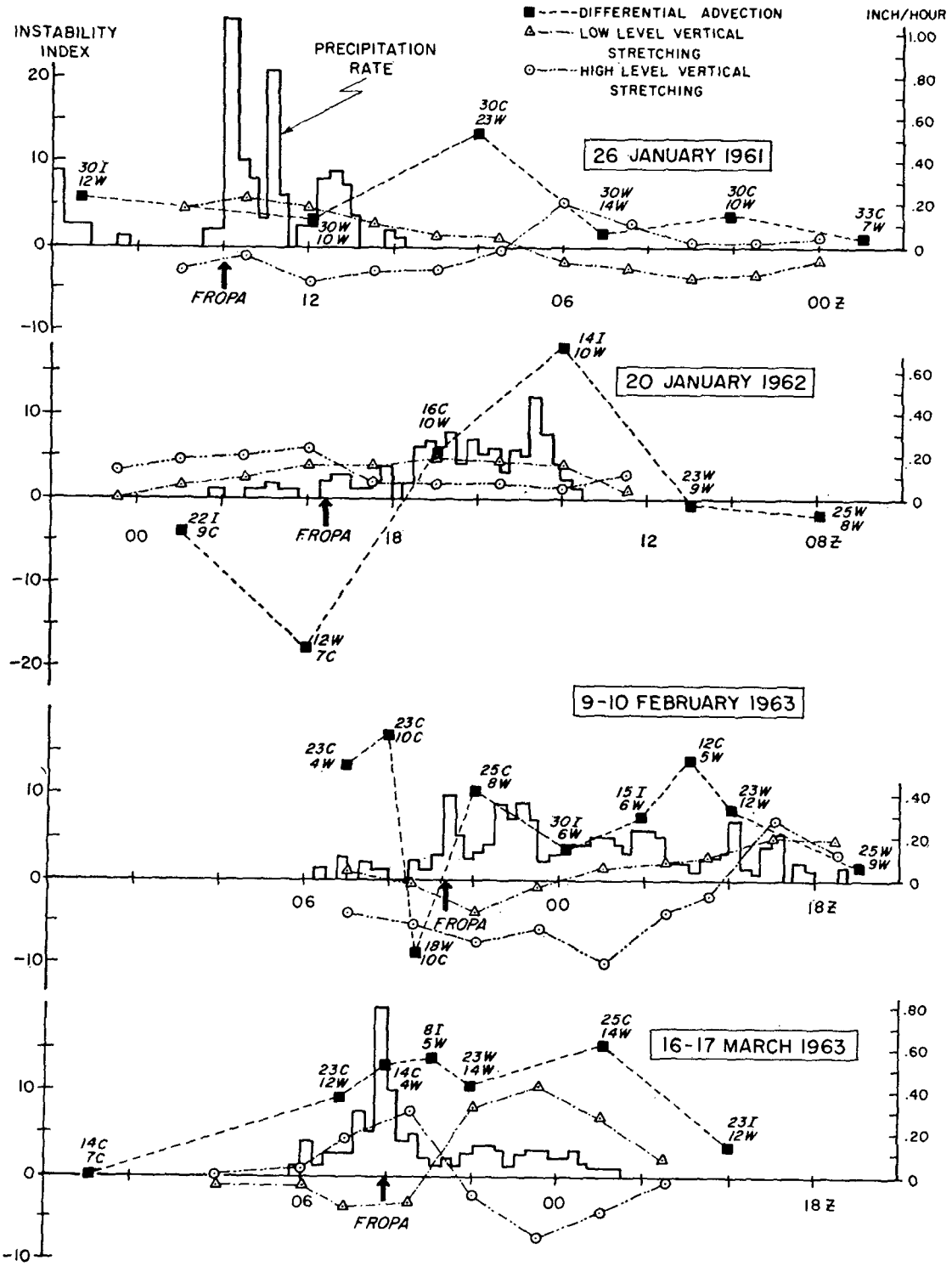

FIG. 10. Precipitation rates (inches per hour) at LAX for four separate storms, together with differential thermal advection and vertical air-mass stretching indices. The index scale for *vertical stretching is in cm* sec^{-1} cb^{-1}. The scale is *arbitrary for differential advection*, but with positive values denoting destabilizing effect. The numbers by each black square show the height in thousands of feet of the low layer (lower number) and upper layer thermal advection with the type by *W* (warm), *C* (cold), and *I* (indifferent).

existing air-mass stability. The overall effect upon the air-mass convection processes can be visualized this way: prior to the onset of precipitation, the vertical stretching will tend to destabilize the more or less moist, stable air mass in advance of the storm precipitation zone. The lapse rate steepens further beyond neutral stability with the sudden onset of pronounced differential thermal advection resulting in marked convective activity, as manifested in increased precipitation. Once instability is realized, a quasi-steady state lapse rate develops which depends upon the balance maintained between the destabilizing effect of the differential advection and the stabilizing effect of convective overturning and, at times, of vertical air-mass stretching.

5. Summary

The classical extratropical cyclone model explains the presence of cloud forms and precipitation primarily in terms of broad scale and relatively gentle lifting of air masses over frontal surfaces. Vertical velocity computations by numerical prediction methods, as based upon the standard data-grid network, support this view. However, the analysis of more detailed aerological and precipitation data presented herein indicates that a much more complex pattern of vertical motion actually exists, which leads to less uniform precipitation distribution.

Of particular interest is the occurrence of organized convection bands within storm systems. The numerous cases analyzed by the authors, of which some are described here, have led to their opinion that these mesoscale organizations of convective activity are common features within extratropical storms. The typical bands are 20 to 40 miles wide, centered 30 to 60 miles apart, and are trackable over a period of at least three hours or some 100 miles. They appear to be oriented along the shear vector between the upper convective cloud region and the adjacent layer above, while steered along a direction of the low-level shear vector. The increased cellular convective activity within these mesoscale bands, associated primarily with the destabilizing effects upon the air mass produced by increases in differential thermal advection, is considered to play an important role in the overall balance of the water, heat and energy budget of extratropical storms.

Acknowledgments. The authors are grateful to the various agencies in and around Santa Barbara for their active participation in the data collection program. In particular, we wish we could acknowledge by name the many individuals at the Pacific Missile Range Weather Center at Point Mugu and their units at Point Arguello and San Nicolas Island, the U. S. Weather Bureau's rawinsonde station at Santa Monica and the forecast center at Los Angeles International Airport, and the U. S. Coast Guard, Santa Barbara group, for their excellent cooperation and support in this program. Furthermore, we are grateful to the U. S. Weather Bureau's Hydrological Services at Sacramento for making available a number of recording raingages for this project.

We wish to note the welcome constructive criticism of several colleagues at Aerometric Research Inc. and to thank Miss Leona Nelken for performing the data computations, Mrs. O. Joyce Shea for preparation of the figures, and Mrs. Louise E. d'Argastel for typing the manuscript.

REFERENCES

Appleby, J. F., 1954: Trajectory method of making short-range forecasts of differential temperature advection, instability, and moisture. *Mon. Wea. Rev.*, **82**, 320–334.

Boucher, R. J., and R. Wexler, 1961: The motion and predictability of precipitation lines. *J. Meteor.*, **18**, 160–171.

Chapman, W. T., and J. A. Carr, 1952: Heavy rainfall over Northeastern Wyoming and Southern Montana, May 21, 1952. *Mon. Wea. Rev.*, **80**, 88–93.

Clarke, R. H., 1961: Meso-structure of dry cold fronts over featureless terrain. *J. Meteor.*, **18**, 715–735.

Harper, W. G., and J. G. D. Beimers, 1958: Movement of precipitation belts. *Quart. J. R. meteor. Soc.*, **84**, 242–249.

Kuettner, J., 1959: The band structure of the atmosphere. *Tellus*, **11**, 267–294.

Malkus, J. S., 1963: Cloud patterns over tropical oceans. *Science*, **141**, 767–778.

Middleton, W. E., 1947: *Meteorological instruments.* Toronto, The University of Toronto Press, p. 118.

Miller, J. E., 1955: Intensification of precipitation by differential advection. *J. Meteor.*, **12**, 472–477.

Showalter, A. K., 1944: An approach to quantitative forecasting of precipitation. *Bull. Amer. meteor. Soc.*, **25**, 137–142.

Smith, C. D., Jr., 1950: The intense Pacific Coast storms of October 26–28, 1950. *Mon. Wea. Rev.*, **78**, 191–195.

Winston, J. S., and L. Tourville, 1961: Cloud structure of an occluded cyclone over the Gulf of Alaska as viewed by TIROS I. *Bull. Amer. meteor. Soc.*, **42**, 151–165.